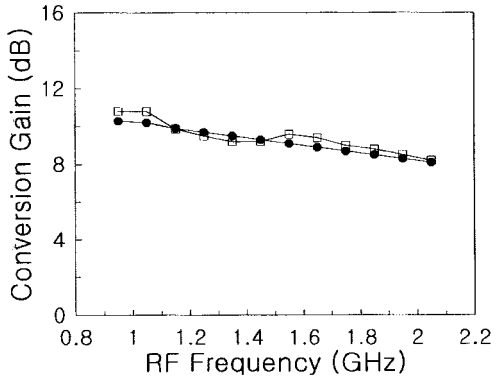

Fig. 5. Comparison of experimental (□) and simulated (•) results for MMIC mixer performance.

MESFET from Kukje has been modeled and a monolithic-microwave-integrated-circuit (MMIC) mixer has been designed and tested for PCS applications. Fig. 5 shows the measured and simulation results of the conversion gain for the frequency range from 0.95 to 2.05 GHz. The maximum conversion-gain difference is less than 1 dB.

IV. Conclusion

In this paper, a very simple new-channel-current model has been proposed, which can represent the frequency-dispersion effects due to traps, channel temperature effect, and higher order derivative terms of $I_{\rm ds}$. The derivative terms are important for predicting nonlinear circuit performance. The model parameters are extracted from the pulsed *I–V* measurements at several ambient temperatures and quiescent bias points. The extraction procedure is straightforward and simple. In order to validate this model, a large-signal model has been extracted for OKI KGF-1284 and Kukje MESFET. The extracted large-signal MESFET models have been implemented using SDD in HP-EEsof MDS. By comparing the pulsed *I–V* and S-parameter measurements with simulation results, the accuracy of this model was verified. This model has also been applied to the design of nonlinear circuits such as power amplifiers and mixers. The harmonic-balance simulations with the proposed model and the experimental results for fabricated circuits confirm the accuracy of the proposed modeling.

References

[1] M. Paggi, P. H. Williams, and J. M. Borrego, "Nonlinear GaAs MESFET modeling using pulsed gate measurements," *IEEE Trans. Microwave Theory Tech.*, vol. 36, pp. 1593–1597, Dec. 1988.

[2] T. Fernandez, Y. Newport, J. M. Zamanillo, A. Tazon, and A. Mediavilla, "Modeling of operating point nonlinear dependence of Ids characteristics from pulsed measurements in MESFET transistors," in *23rd European Microwave Conf. Dig.*, Madrid, Spain, Sept. 1993, pp. 518–521.

[3] F. Filicori, G. Vanni, A. Mediavilla, and A. Tazon, "Modeling of deviations between static and dynamic drain characteristics in GaAs FET's," in *23rd European Microwave Conf. Dig.*, Madrid, Spain, Sept. 1993, pp. 454–457.

[4] F. Filicori, G. Vanni, A. Santarelli, A. Mediavilla, A. Tazon, and Y. Newport, "Empirical modeling of low-frequency dispersive effects due to traps and thermal phenomena in III-V FET's," *IEEE Trans. Microwave Theory Tech.*, vol. 43, pp. 2972–2981, Dec. 1995.

[5] T. Fernandez, Y. Newport, J. M. Zamanillo, A. Tazon, and A. Mediavilla, "Extracting a bias-dependent large signal MESFET model from pulsed *I/V* measurements," *IEEE Trans. Microwave Theory Tech.*, vol. 44, pp. 372–378, Mar. 1996.

[6] P. H. Ladbrooke and S. R. Blight, "Low-field low-frequency dispersion of transconductance in GaAs MESFET's with implications for other rate-dependent anomalies," *IEEE Trans. Electron Devices*, vol. 35, pp. 257–267, 1988.

[7] J. A. Reynoso-Hernandez and J. Graffeuil, "Output conductance frequency dispersion and low-frequency noise in HEMT's and MESFET's," *IEEE Trans. Microwave Theory Tech.*, vol. 37, pp. 1478–1481, Sept. 1989.

[8] J. M. Golio, M. G. Miller, G. N. Maracas, and D. A. Johnson, "Frequency-dependent electrical characteristics of GaAs MESFET's," *IEEE Trans. Electron Devices*, vol. 37, pp. 1217–1227, May 1990.

[9] S. A. Mass and D. Neilson, "Modeling MESFET's for Intermodulation Analysis of Mixers and Amplifiers," *IEEE Trans. Microwave Theory Tech.*, vol. 38, pp. 1964–1971, Dec. 1990.

[10] ____, "Modeling GaAs MESFET's for intermodulation analysis," *Microwave J.*, pp. 295–300, May 1991.

[11] J. C. Pedro and J. Perez, "A novel non-linear GaAs FET model for intermodulation analysis in general purpose harmonic-balance simulators," in *23rd European Microwave Conf. Dig.*, Madrid, Spain, Sept. 1993, pp. 714–716.

[12] W. R. Curtice, "GaAs MESFET modeling and nonlinear CAD," *IEEE Trans. Microwave Theory Tech.*, vol. 36, pp. 220–230, Feb. 1988.

[13] J. Rodriguez-Tellez, K. A. Mezher, O. M. Conde Portilla, and J. C. Luengo Patrocinio, "A highly accurate microwave nonlinear MESFET model," *Microwave J.*, pp. 280–285, May 1993.

Two-Port Scattering at an Elliptic-Waveguide Junction

Kin-Lung Chan and Sunil R. Judah

***Abstract*— A concentric waveguide junction consisting of an elliptic waveguide has been formulated using the mode-matching method. The formulation is a generalized solution of the problem such that the second waveguide, which forms the junction, can be any regular shape in cross section. Exact closed-form expressions for computing the coupling integrals have been obtained from the generalized formulation. As a special case of the general solution, the expressions for evaluating the coupling integrals of rectangular-to-elliptic, circular-to-elliptic, and elliptic-to-elliptic waveguide junction are given. Theoretical results compare well with the experimental and published results.**

***Index Terms*—Elliptic waveguide, mode-matching method, waveguide junction.**

I. Introduction

One of the advantages of using elliptic waveguides is that the spectral separation between propagating modes can be varied by changing the eccentricity. It then prevents mode coupling due to imperfection of waveguide curvature or waveguide bending, as happens in a circular waveguide. The desired propagating mode, therefore, can be preserved. The use of elliptic waveguides is becoming more popular in microwave systems and the behavior of transition from waveguides having different geometries to elliptic waveguides becomes important.

The formulations of waveguide discontinuities involving rectangular or circular waveguides have been well documented in the literature [1]–[5]. Recently, Matras *et al*. [6] studied the scattering

Manuscript received June 13, 1996; revised March 17, 1997.

The authors are with the Department of Electronic Engineering, University of Hull, Hull, HU6 7RX U.K.

Publisher Item Identifier S 0018-9480(97)05384-2.

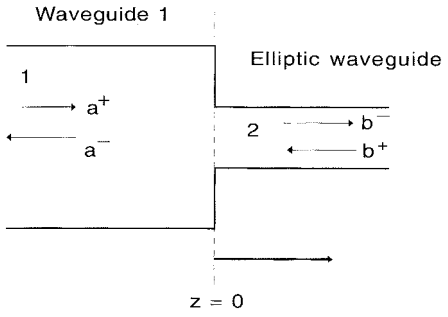

Fig. 1. Waveguide 1 to elliptic-waveguide junction.

characteristic of a waveguide junction formed by two concentric-confocal-elliptic waveguides. However, the discontinuity involving elliptic waveguides has received scant attention. In this paper, the mode-matching method is used to investigate the scattering characteristic of different waveguide junctions formed by an elliptic waveguide and commonly used waveguide geometries. The waveguide junctions considered in this paper are: 1) rectangular-to-elliptic; 2) circular-to-elliptic; and 3) confocal and nonconfocal elliptic-to-elliptic. It is shown in the a later section that all these types of waveguide-junction problems can be derived from a generalized formulation and share the same form of coupling-coefficient expressions.

The mode-matching technique is found to be an elegant method in tackling waveguide-junction problems. It has been widely employed in determining discontinuity characteristics in waveguide junctions. By expanding the modal fields in the waveguides at both sides of the junction, and then imposing the boundary condition to the modal fields at the junction plane, the generalized scattering matrix of the junction can be evaluated.

In the generalized formulation of the waveguide-junction problem, the modal fields are expressed on both sides of the junction in terms of Mathieu functions, which leads to exact closed-form expressions for computing the coupling integrals. All the terms in the coupling coefficients can then be analytically evaluated with only the exception of the elliptic-waveguide normalization constant, which has to be evaluated numerically. As special cases for the generalized formulation, expressions are given in Section IV to evaluate the coupling coefficients of the junction formed by an elliptic waveguide and three different waveguide geometries—namely rectangular, circular, and elliptic.

II. General Waveguide-Junction Formulation Using the Mode-Matching Method

The configuration of the waveguide-junction problem addressed in this paper is shown in Fig. 1. The junction is formed by two air-filled waveguides, waveguide 1 (rectangular, circular, or elliptic) and waveguide 2 (elliptic), which are concentrically joined at the $z = 0$ plane. In this paper, only the case where waveguide 1 is larger than the elliptic waveguide is studied, i.e., the elliptic cross section is completely enclosed by the cross-sectional area of the other waveguide.

The entire waveguide-junction problem can be formulated by using the generalized scattering-matrix technique [7]. The modal coefficients of the waveguide modes a, b are related as

$$\begin{bmatrix} a^- \\ b^- \end{bmatrix} = \begin{bmatrix} [S_{11}] & [S_{12}] \\ [S_{21}] & [S_{22}] \end{bmatrix} \begin{bmatrix} a^+ \\ b^+ \end{bmatrix} \tag{1}$$

where the superscript $+$ and $-$ represent the transmitted and reflected wave, respectively. $[S_{ij}]$ in (1) are submatrices representing the modal scattering coefficients of the ith to jth guide, and these are the unknowns that need to be determined.

To determine the modal scattering coefficients, the mode-matching technique can be employed. It basically requires expanding the electric and magnetic field in both waveguides in terms of their respective waveguide modes, followed by matching the field at the junction. Details of the mode-matching procedure for computing the scattering coefficients of a waveguide junction are well-documented in the literature [1], [2], [8], and will not be repeated here. Consequently, only the procedures covering the derivation of the coupling coefficients are presented in this paper.

The coupling matrix $[M]$, in the E-field mode-matching equation [1], is defined as

$$[M] = \begin{bmatrix} [\mathbf{H}] & [\mathbf{K}] \\ [\mathbf{G}] & [\mathbf{F}] \end{bmatrix} \tag{2}$$

where $[\mathbf{H}]$ represents the TE–TE mode-coupling submatrix, $[\mathbf{K}]$ for TE–TM mode coupling, $[\mathbf{G}]$ for TM–TE mode coupling, and $[\mathbf{F}]$ for TM–TM mode coupling.

The elements of the submatrices $[\mathbf{H}]$–$[\mathbf{F}]$ in (2) are the coupling coefficients, which are evaluated by the following integrals:

$$\mathbf{H}_{\mathrm{mnpq}} = \int_{S_e} \vec{\psi}^h_{pq} \cdot \vec{\phi}^h_{mn}\, dS \tag{3}$$

$$\mathbf{K}_{\mathrm{mnpq}} = \int_{S_e} \vec{\psi}^e_{pq} \cdot \vec{\phi}^h_{mn}\, dS \tag{4}$$

$$\mathbf{G}_{\mathrm{mnpq}} = \int_{S_e} \vec{\psi}^h_{pq} \cdot \vec{\phi}^e_{mn}\, dS \tag{5}$$

$$\mathbf{F}_{\mathrm{mnpq}} = \int_{S_e} \vec{\psi}^e_{pq} \cdot \vec{\phi}^e_{mn}\, dS \tag{6}$$

where S_e is the cross-sectional area of the elliptic waveguide, $\vec{\phi}_{mn}$ and $\vec{\psi}_{pq}$ are, respectively, the transverse-modal electric field in waveguide 1 and the elliptic waveguide. The superscripts h, e, attached to the modal fields, denote TE and TM modes, respectively. The boundary condition for the electric field at $z = 0$ plane has been incorporated in (3)–(6). Consequently, the integrations are performed over the cross-sectional area of the smaller elliptic waveguide.

Since the solution of the wave equation in waveguide 1 is separable in the transverse coordinates, the field can be set up in the usual manner in terms of TE and TM modes. For TM modes, the axial electric-field component E_z, in the region $z < 0$, can be written as

$$E_z = \sum_m \sum_n \varphi_{mn}(\zeta_1, \zeta_2) \tag{7}$$

where ζ_1 and ζ_2 are the transverse coordinates in waveguide 1 and φ is the modal-field function. φ_{mn} are the normal-mode functions for the particular waveguide—for instance, trigonometric functions for rectangular waveguides. However, for this problem, it is convenient to expand all the modal fields in terms of Mathieu functions. It is well known that Mathieu functions are orthogonal and, therefore, form an orthogonal basis set for the modal-field function φ_{mn}. φ_{mn} can then be expressed as a Mathieu series, and E_z can be written as

$$E_z = \sum_{m,n}^{\infty} \sum_{k=0}^{\infty} \Lambda_{mn,k} \begin{Bmatrix} Je_k(h_{mn}, u) Se_k(h_{mn}, v) \\ Jo_k(h_{mn}, u) So_k(h_{mn}, v) \end{Bmatrix} \tag{8}$$

where $\Lambda_{mn,k}$ are the Mathieu series coefficients, $Ji_k(h_{mn}, u)$ is the first-kind radial Mathieu function, and $Si_k(h_{mn}, v)$ is the first-kind circumferential Mathieu function, in which $i = e$ or o denote the

even or odd mode, respectively. The argument h_{mn} in (8) is

$$h_{mn} = l\beta_{mn}$$

where l is the focal length of the elliptic coordinate system and β_{mn} is the TM-mode cutoff wavenumber in waveguide 1. For TE modes, a very similar expression can be obtained for the axial magnetic-field component H_z.

Then, from Maxwell equations, the transverse electric-field components in waveguide 1, in elliptic coordinate system $\hat{u}$, $\hat{v}$, are

$$\vec{\phi}^h_{mn} = \frac{N^h_{mn}}{W}\left[\hat{u} - \sum_{k=0}^{\infty}\Lambda^h_{mn,k}\begin{Bmatrix} Je_k(h'_{mn},u)Se'_k(h'_{mn},v) \\ Jo_k(h'_{mn},u)So'_k(h'_{mn},v)\end{Bmatrix} + \hat{v}\sum_{k=0}^{\infty}\Lambda^h_{mn,k}\begin{Bmatrix} Je'_k(h'_{mn},u)Se_k(h'_{mn},v) \\ Jo'_k(h'_{mn},u)So_k(h'_{mn},v)\end{Bmatrix}\right] \quad (9)$$

$$\vec{\phi}^e_{mn} = \frac{N^e_{mn}}{W}\left[\hat{u}\sum_{k=0}^{\infty}\Lambda^e_{mn,k}\begin{Bmatrix} Je'_k(h_{mn},u)Se_k(h_{mn},v) \\ Jo'_k(h_{mn},u)So_k(h_{mn},v)\end{Bmatrix} + \hat{v}\sum_{k=0}^{\infty}\Lambda^e_{mn,k}\begin{Bmatrix} Je_k(h_{mn},u)Se'_k(h_{mn},v) \\ Jo_k(h_{mn},u)So'_k(h_{mn},v)\end{Bmatrix}\right] \quad (10)$$

where $'$ denotes the derivative of the function with respect to its coordinate argument, N_{mn}'s are the normalization constants of waveguide 1 and

$$W = l\sqrt{\cosh^2(u) - \cos^2(v)}.$$

The field components in (9) and (10) can be even or odd modes depending on the incident field in the waveguide.

In the elliptic waveguide, the TE-mode electric field is

$$\vec{\psi}^h_{pq} = \frac{C^h_{pq}}{W}[-\hat{u}\{Je_p(h'_{pq},u)Se'_p(h'_{pq},v) + Jo_p(h'_{pq},u)So'_p(h'_{pq},v)\} + \hat{v}\{Je'_p(h'_{pq},u)Se_p(h'_{pq},v) + Jo'_p(h'_{pq},u)So_p(h'_{pq},v)\}] \quad (11)$$

while the TM-mode electric field is

$$\vec{\psi}^e_{pq} = \frac{C^e_{pq}}{W}[\hat{u}\{Je'_p(h_{pq},u)Se_p(h_{pq},v) + Jo'_p(h_{pq},u)So_p(h_{pq},v)\} + \hat{v}\{Je_p(h_{pq},u)Se'_p(h_{pq},v) + Jo_p(h_{pq},u)So'_p(h_{pq},v)\}] \quad (12)$$

where the C_{pq}'s are the normalization constants for the modes in the elliptic waveguide.

The elliptic aperture problem is a straightforward extension of the junction problem. It can be considered as two waveguide junctions connected through a section of elliptic waveguides. The configuration of the junction with aperture thickness of ι is shown in Fig. 2. The detailed formulation of such a problem is also available in [1].

III. Evaluation of Coupling Integrals

The evaluation of the coupling integrals is the crucial part in formulating waveguide-discontinuity problems. It is always preferable to compute the coupling integrals in closed-form expressions such that time-consuming numerical integrations can be avoided. In this section, it is shown that the four types of coupling integrals presented in (3)–(6) can be evaluated in closed form.

To simplify the notation in this section, J_{pq}, S_{pq} is used to denote the radial- and circumferential-type modal functions in the elliptic waveguide, while J_{mn}, S_{mn} represent the modal function in waveguide 1. It is also understood that the summation over k is always associated with J_{mn}, S_{mn}.

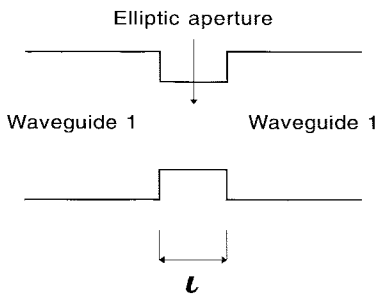

Fig. 2. An elliptic aperture with thickness of ι placed between two waveguide 1's.

A. TE–TM-Mode and TM–TE-Mode Coupling Coefficient

The integral to evaluate TE–TM coupling-coefficient, $\mathbf{K}_{\mathrm{mnpq}}$, and TM–TE coupling-coefficent $\mathbf{G}_{\mathrm{mnpq}}$, has the form

$$\mathbf{C}^I_{\mathrm{mnpq}} = \sum_{k=0}^{\infty}\Lambda_{mn,k}\left\{\int_0^{2\pi} S'_{mn}S_{pq}\,dv\int_0^{u_o} J_{mn}J'_{pq}\,du - \int_0^{2\pi} S_{mn}S'_{pq}\,dv\int_0^{u_o} J'_{mn}J_{pq}\,du\right\}. \quad (13)$$

Here, the modal function has been generalized as S_{xx} and J_{xx}, but, they are either TE or TM modal fields depending on the type of the coupling integral $\mathbf{C}^I_{\mathrm{mnpq}}$.

Equation (13) can be easily simplified using integration by parts as

$$\mathbf{C}^I_{\mathrm{mnpq}} = \sum_{k=0}^{\infty}\Lambda_{mn,k}\left\{-[J_{mn}J_{pq}]_0^{u_o}\int_0^{2\pi} S'_{mn}S_{pq}\,dv + \mathbf{Ia}\right\} \quad (14)$$

where

$$\mathbf{Ia} = \int_0^{u_o} J_{mn}J'_{pq}\,du\left(\int_0^{2\pi} S'_{mn}S_{pq}\,dv + \int_0^{2\pi} S_{mn}S'_{pq}\,du\right).$$

Furthermore, for the integrals involving circumferential-type Mathieu functions

$$\int_0^{2\pi} S'_{mn}S_{pq}\,dv + \int_0^{2\pi} S_{mn}S'_{pq}\,du = [S_{mn}S_{pq}]_0^{2\pi} = 0 \quad (15)$$

then $\mathbf{Ia} = 0$ and (14) becomes

$$\mathbf{C}^I_{\mathrm{mnpq}} = -\sum_{k=0}^{\infty}\Lambda_{mn,k}\left\{[J_{mn}J_{pq}]_0^{u_o}\int_0^{2\pi} S'_{mn}S_{pq}\,dv\right\}. \quad (16)$$

At this point, it should be recalled that the modal functions J and S consist of even and odd modes. However, by applying the orthogonal property of Mathieu functions to (16), it is found that the coupling exists only between even-to-odd and odd-to-even modes. In addition, because of the properties of radial-type Mathieu function

$$\begin{cases} J(0) = 0, & \text{for odd type of } J \\ J'(0) = 0, & \text{for even type of } J\end{cases} \quad (17)$$

then (16) vanishes at the limit when $u = 0$.

To evaluate $\mathbf{K}_{\mathrm{mnpq}}$, TM-mode boundary conditions are imposed for the elliptic-waveguide $J_{pq}(u_o) = 0$ on (16). Consequently, $\mathbf{K}_{\mathrm{mnpq}}$ is found to be equal to 0 for all pq's, which is a well-known result for the TE-to-TM coupling [9].

For $\mathbf{G}_{\mathrm{mnpq}}$, using the conventional notation, it can be written as

$$\mathbf{G}_{\mathrm{mnpq}} = \pm N^e_{mn} C^h_{pq} \pi \sum_{k=0}^{\infty} \Lambda^e_{mn,k} Is'_k \times \begin{Bmatrix} Je_k(h_{mn}, u_o) & Jo_p(h'_{pq}, u_o) \\ Jo_k(h_{mn}, u_o) & Je_p(h'_{pq}, u_o) \end{Bmatrix} \tag{18}$$

where

$$Is'_k = \sum_{s=0}^{\infty} s A^{mn}_s A^{pq}_s$$

and A^{mn}_s and A^{pq}_s are the coefficients of the Mathieu function S_{mn} and S_{pq}, respectively.

B. TE–TE- and TM–TM-Mode Coupling Coefficients

For TE–TE coupling-coefficients $\mathbf{H}_{\mathrm{mnpq}}$, and TM–TM coupling-coefficent $\mathbf{F}_{\mathrm{mnpq}}$, the common form of the integral is

$$\mathbf{C}^{\mathrm{II}}_{\mathrm{mnpq}} = \sum_{k=0}^{\infty} \Lambda_{mn,k} \left\{ \int_0^{2\pi} S'_{mn} S'_{pq}\, dv \int_0^{u_o} J_{mn} J_{pq}\, du + \int_0^{2\pi} S_{mn} S_{pq}\, dv \int_0^{u_o} J'_{mn} J'_{pq}\, du \right\}. \tag{19}$$

Employing the relationship of (51), given in the Appendix, and after some rearrangement of terms, (19) becomes

$$\mathbf{C}^{\mathrm{II}}_{\mathrm{mnpq}} = \sum_{k=0}^{\infty} \Lambda_{mn,k} \left\{ \mathbf{Ib} \int_0^{u_o} J_{mn} J_{pq}\, du + \int_0^{2\pi} S_{mn} S_{pq}\, dv \times \left([J'_{mn} J_{pq}]_0^{u_o} - \frac{h^2_{mn}}{h^2_{pq} - h^2_{mn}} \times [J'_{pq} J_{mn} - J'_{mn} J_{pq}]_0^{u_o} \right) \right\} \tag{20}$$

where

$$\mathbf{Ib} = \frac{a_{pq} h^2_{mn} - a_{mn} h^2_{pq}}{h^2_{pq} - h^2_{mn}} \int_0^{2\pi} S''_{mn} S''_{pq}\, dv - \int_0^{2\pi} S_{mn} S_{pq}\, dv.$$

As shown in the Appendix, $\mathbf{Ib}$ is equal to 0, thus, (20) reduces to

$$\mathbf{C}^{\mathrm{II}}_{\mathrm{mnpq}} = \sum_{k=0}^{\infty} \Lambda_k \left\{ \int_0^{2\pi} S_{mn} S_{pq}\, dv \left(\frac{h^2_{pq}}{h^2_{pq} - h^2_{mn}} [J'_{mn} J_{pq}]_0^{u_o} - \frac{h^2_{mn}}{h^2_{pq} - h^2_{mn}} [J'_{pq} J_{mn}]_0^{u_o} \right) \right\}. \tag{21}$$

Analogous to the analysis of $\mathbf{C}^{\mathrm{I}}_{\mathrm{mnpq}}$, the orthogonal properties of the circumferential-type Mathieu function is applied to (21), then the mode coupling is found to be restricted to even-to-even and odd-to-odd modes only. Furthermore, $\mathbf{C}^{\mathrm{II}}_{\mathrm{mnpq}}$ is equal to 0 at $u = 0$ because of (17).

Lastly, the boundary condition of the elliptic waveguide at $u = u_o$ is attached to (21). After imposing the TE-mode boundary condition $J'_{pq}(u_o) = 0$, one finds

$$\mathbf{H}_{\mathrm{mnpq}} = N^h_{mn} C^h_{pq} \pi \frac{h'^2_{pq}}{h'^2_{pq} - h'^2_{mn}} \sum_{k=0}^{\infty} \Lambda^h_{mn,k} Is_k \times \begin{Bmatrix} Je'_k(h'_{mn}, u_o) & Je_p(h'_{pq}, u_o) \\ Jo'_k(h'_{mn}, u_o) & Jo_p(h'_{pq}, u_o) \end{Bmatrix} \tag{22}$$

where

$$Is_k = \sum_{s=0}^{\infty} \varepsilon_s A^{mn}_s A^{pq}_s.$$

$\varepsilon_s = 2$ when $s = 0$ and $\varepsilon_s = 1$ when $s \neq 0$.

On the other hand, the boundary condition of J_{pq} for the TM mode requires that $J_{pq}(u_o) = 0$. Thus, $\mathbf{F}_{\mathrm{mnpq}}$ reduces to

$$\mathbf{F}_{\mathrm{mnpq}} = N^e_{mn} C^e_{pq} \pi \frac{h^2_{mn}}{h^2_{mn} - h^2_{pq}} \sum_{k=0}^{\infty} \Lambda^e_{mn,k} Is_k \times \begin{Bmatrix} Je_k(h_{mn}, u_o) & Je'_p(h_{pq}, u_o) \\ Jo_k(h_{mn}, u_o) & Jo'_p(h_{pq}, u_o) \end{Bmatrix}. \tag{23}$$

In the above analysis, the integration, with respect to the argument v, is converted into a series summation of the Mathieu coefficient Is_k; this is done as the series converges rapidly. Moreover, due to the highly converging characteristic of the radial-type Mathieu functions, almost 20 terms of the infinite series are more than sufficient to give accurate results. The expressions (18), (22), and (23) are general, and are applicable to any concentric waveguide junction consisting of a smaller elliptic waveguide, provided the axial fields in the larger waveguide can be expressed as a Mathieu series.

IV. Different Geometries to Elliptic Waveguide Junction

In most applications, the dominant mode in a waveguide is of primary interest, therefore, the analysis given in this section considers only the dominant mode incident in the larger waveguide. The evaluation of the S-parameters for higher order incident modes is a trivial extension of what follows. Under this circumstance, the symmetry condition of the dominant mode can be imposed on the modal fields excited at the junction. In addition, the coupling-coefficient expressions arising from the different geometries differ only in the coefficients of the Mathieu series Λ_k, and as is shown in this section, all Λ_k's can be evaluated by simple expressions.

A. Rectangular to Elliptic

The axial magnetic component Hz, excited by the dominant mode of the rectangular waveguide, is given as

$$Hz_{mn} = \sin\left(\frac{m\pi}{a} x\right) \cos\left(\frac{n\pi}{b} y\right) \tag{24}$$

where a and b are the width and height of the rectangular waveguide, $m = \mathrm{odd}$ and $n = \mathrm{even}$. Hz_{mn} can be transformed to elliptical-coordinate arguments (u, v) as [10]

$$Hz_{mn} = \sqrt{8\pi} \sum_{k=0}^{\infty} (-1)^k \frac{Se_{2k+1}(h_{mn}, \theta_{mn})}{Me_{2k+1}(h_{mn})} \times Se_{2k+1}(h_{mn}, v) Je_{2k+1}(h_{mn}, u) \tag{25}$$

where

$$\theta_{mn} = \tan^{-1}\left(\frac{na}{mb}\right)$$
$$h_{mn} = l\sqrt{{k_m}^2 + {k_n}^2}$$
$$k_m = \frac{m\pi}{a}$$
$$k_n = \frac{n\pi}{b}$$

and $Me_n(h_{mn})$ is the normalization constant of the nth-order even-Mathieu function with argument h_{mn}.

When compared with (8) for TE modes, one gets

$$\Lambda^h_{mn,k} = \sqrt{8\pi}(-1)^k \frac{Se_{2k+1}(h_{mn}, \theta_{mn})}{Me_{2k+1}(h_{mn})} \tag{26}$$

where only the even modes with odd order exist.

The axial electric component Ez_{mn} in elliptic coordinates is

$$Ez_{mn} = \sqrt{8\pi}\sum_{k=0}^{\infty}(-1)^k \frac{So_{2k+1}(h_{mn},\theta_{mn})}{Mo_{2k+1}(h_{mn})} \times So_{2k+1}(h_{mn},v)Jo_{2k+1}(h_{mn},u). \quad (27)$$

Ez_{mn} only consists of odd Mathieu functions with odd order, due to the symmetry condition imposed by the dominant mode. In a similar way, the TM mode coefficient $\Lambda^e_{mn,k}$ is obtained as

$$\Lambda^e_{mn,k} = \sqrt{8\pi}(-1)^k \frac{So_{2k+1}(h_{mn},\theta_{mn})}{Mo_{2k+1}(h_{mn})}. \quad (28)$$

The normalization constant for the rectangular-waveguide mode, N_{mn}, is

$$N_{mn} = \frac{2}{\sqrt{ab\left(k_n{}^2 + \sigma k_m{}^2\right)}} \quad (29)$$

with $\sigma = 2$, if $n = 0$, and $\sigma = 1$, when $n \neq 0$.

Using (26), (28), and (29) in (22)–(23), the coupling coefficients of a rectangular-to-elliptic waveguide junction are obtained directly.

B. Circular to Elliptic

Replacing the rectangular waveguide with a circular waveguide, the axial magnetic component Hz of the circular waveguide is given as

$$Hz_{mn} = J_m(\beta'_{mn} r)\cos(m\theta) \quad (30)$$

where $J_m()$ is the Bessel function. Due to the symmetry condition of the dominant TE_{11} mode in the circular waveguide, only odd m's are considered and Hz_{mn} in elliptic coordinates becomes [11]

$$Hz_{mn} = \sqrt{2\pi}\sum_{k=0}^{\infty}\left(j^{2k+1-m}\right)\frac{Ae_m(2k+1,h'_{mn})}{Me_{2k+1}(h'_{mn})} \times Se_{2k+1}(h'_{mn},v)Je_{2k+1}(h'_{mn},u). \quad (31)$$

where

$$h'_{mn} = l\beta'_{mn}$$

β'_{mn} is the TE-mode cutoff wavenumber of the circular waveguide and $Ae_s(k,h_{mn})$ represents the sth coefficient for the even-mode Mathieu function with order k and argument h_{mn}.

Comparing (31) with (8), for the TE mode, one has

$$\Lambda^h_{mn,k} = \sqrt{2\pi}\left(j^{2k+1-m}\right)\frac{Ae_m(2k+1,h'_{mn})}{Me_{2k+1}(h'_{mn})}. \quad (32)$$

The TM-mode coefficient is found to be

$$\Lambda^e_{mn,k} = \sqrt{2\pi}\left(j^{2k+1-m}\right)\frac{Ao_m(2k+1,h_{mn})}{Mo_{2k+1}(h_{mn})} \quad (33)$$

where

$$h_{mn} = l\beta_{mn}$$

and β_{mn} are the TM-mode cutoff wavenumbers of the circular waveguide.

The normalization constants for the TE mode is

$$N^h_{mn} = \frac{\sqrt{2/\pi}}{J_m(\beta'_{mn}R)\sqrt{\beta'_{mn}R^2 - m^2}} \quad (34)$$

and for the TM mode is

$$N^e_{mn} = \frac{\sqrt{2/\pi}}{\beta_{mn}RJ_m(\beta_{mn}R)} \quad (35)$$

where R is the radius of the circular waveguide.

Again, using (32)–(35) in (22)–(23), the coupling coefficients for circular–elliptic waveguide junction can be evaluated.

TABLE I
CONVERGENCE OF S11 FOR THE RECTANGULAR-TO-ELLIPTIC WAVEGUIDE JUNCTION AT 12 GHz. RECTANGULAR WAVEGUIDE: $a = 22.86$, MM $b = 10.16$ MM. ELLIPTIC WAVEGUIDE: MAJOR AXIS = 15 MM AND MINOR AXIS = 7 MM

Highest cutoff wavenumber	Rectangular waveguide No. of modes		Elliptic waveguide No. of modes		Reflection Coefficient S11	
hpq	TE	TM	TE	TM	Magnitude	Phase
12	18	11	7	3	0.6213	42.75
15	28	20	11	6	0.6247	44.39
20	47	36	19	11	0.6249	44.40
25	73	59	27	19	0.6250	44.48

C. Elliptic to Elliptic

The last example presented here is the elliptic-to-elliptic waveguide-junction problem. For this, the z-component of the magnetic field Hz in elliptic coordinates is given as [12]

$$Hz_{mn} = Je_{2m+1}(\tilde{h}'_{mn},\tilde{u})Se_{2m+1}(\tilde{h}'_{mn},\tilde{v}) \quad (36)$$

where $\tilde{u}$ and $\tilde{v}$ are the coordinates in the larger elliptic waveguide. Only even modes with odd order are considered, as TE_{11} is the dominant mode.

In general, $(\tilde{u},\tilde{v})$ is different from the elliptic coordinates in the smaller elliptic-waveguide (u,v), except when the two elliptic waveguides are confocal. Therefore, the elliptic-to-elliptic waveguide-junction problem can be considered as two separate cases—namely, a junction formed by confocal and nonconfocal elliptic waveguides. In the former case, the coordinate systems at both sides of the junction coincide, i.e., $\tilde{u} = u$ and $\tilde{v} = v$, while in the latter case, different elliptic coordinate systems exist in each waveguide. Despite the fact that there are two different cases for an elliptic-to-elliptic waveguide junction, corresponding to the confocal and nonconfocal cases, both can be solved by applying the generalized formulation.

For the confocal elliptic-to-elliptic waveguide-junction problem, the form of Hz in (36) can be applied directly to the mode-matching method as it stands. In the larger elliptic waveguide, each modal field is represented by a single order of the Mathieu function; hence, the summation series of k in (22)–(23) vanishes and Λ_k becomes 1. In addition, h_{mn} in (22)–(23) are simply the cutoff wavenumbers of the larger elliptic waveguide, $\tilde{h}_{mn}$. As expected, with these conditions applied, the expressions given in the previous section produce the same coupling-coefficient expressions as in [6].

For the nonconfocal waveguide junction, the modal fields in the larger elliptic waveguide need to be transformed to the elliptic coordinates in the smaller waveguide. By using the addition theorem of Mathieu functions [13], Hz in (36) can be expressed in the (u,v) coordinate as

$$Hz_{mn} = \sum_{k=0}^{\infty}\frac{\pi(-1)^{k-m}}{Me_{2k+1}(h'_{mn})} \times \left\{\sum_{s=0}^{\infty}Ae_{2s+1}(2m+1,\tilde{h}'_{mn})Ae_{2s+1}(2k+1,h'_{mn})\right\} \times Je_{2k+1}(h'_{mn},u)Se_{2k+1}(h'_{mn},v) \quad (37)$$

where

$$h'_{mn} = \frac{l_2}{l_1}\tilde{h}'_{mn}$$

and l_1 and l_2 are the focal length of the elliptic coordinate system in the larger and the smaller elliptic waveguides, respectively.

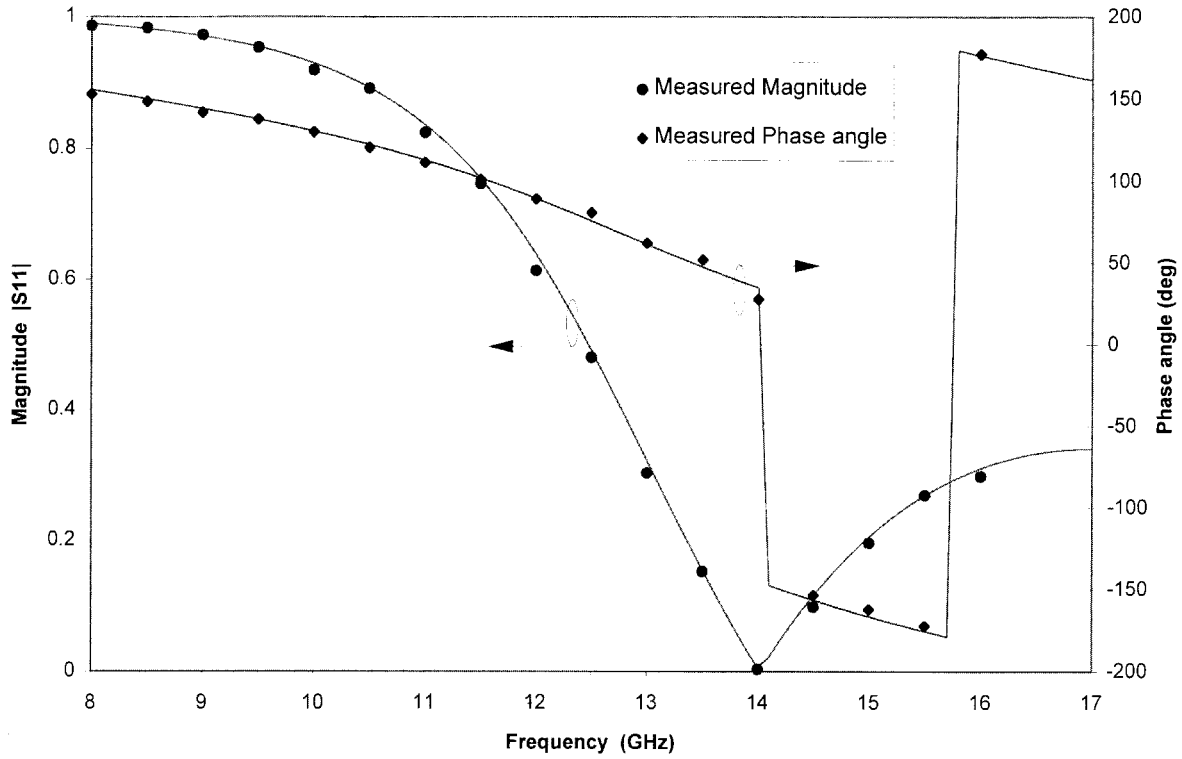

Fig. 3. Calculated and measured reflection coefficient of an elliptic aperture (major = 15 mm, minor = 7 mm) with thickness of 7.5 mm inside a X-band rectangular waveguide.

Following the procedure described in Section B, and comparing (37) with (8), one gets for TE modes

$$\Lambda^h_{mn,k} = \frac{\pi(-1)^{k-m}}{Me_{2k+1}(h'_{mn})} \sum_{s=0}^{\infty} Ae_{2s+1}(2m+1, \tilde{h}'_{mn}) \times Ae_{2s+1}(2k+1, h'_{mn}) \tag{38}$$

and for TM modes

$$\Lambda^e_{mn,k} = \frac{-\pi(-1)^{k-m}}{Mo_{2k+1}(h_{mn})} \sum_{s=0}^{\infty} Ao_{2s+1}(2m+1, \tilde{h}_{mn}) \times Ao_{2s+1}(2k+1, h_{mn}) \tag{39}$$

where

$$h_{mn} = \frac{l_2}{l_1}\tilde{h}_{mn}.$$

For the TE mode, the normalization constant of an elliptic waveguide is

$$N^h_{mn} = \left[\pi\left\{\sum_{s=0}^{\infty}(2s+1)^2(Ae_{2s+1}(2k+1,h'_{mn}))^2 \times \int_0^{u_o}(Je_{2k+1}(h'_{mn},u))^2\,du + \sum_{s=0}^{\infty}(Ae_{2s+1}(2k+1,h'_{mn}))^2 \times \int_0^{u_o}(Je'_{2k+1}(h'_{mn},u))^2\,du\right\}\right]^{-\frac{1}{2}} \tag{40}$$

while for the TM mode

$$N^e_{mn} = \left[\pi\left\{\sum_{s=0}^{\infty}(Ao_{2s+1}(2k+1,h_{mn}))^2 \times \int_0^{u_o}(Jo'_{2k+1}(h_{mn},u))^2\,du + \sum_{s=0}^{\infty}(2s+1)^2(Ao_{2s+1}(2k+1,h_{mn}))^2 \times \int_0^{u_o}(Jo_{2k+1}(h_{mn},u))^2\,du\right\}\right]^{-\frac{1}{2}}. \tag{41}$$

In (40) and (41), the integrals involving the coordinate variable v have been converted into a summation series of Mathieu coefficients. Thus, only the integrals which involve the radial-type Mathieu functions are the ones that have to be evaluated numerically.

Once again, (38)–(41), together with (22)–(23), provide all the expressions required to evaluate the coupling coefficients of a nonconfocal elliptic–elliptic waveguide junction.

V. Numerical Convergence

One of the key concerns about the mode-matching technique is relative convergence. The ratio of modes used on both sides of the junction affects the computation accuracy [7], [14]. To avoid the relative-convergence problem, the mode-ratio scheme is employed such that the cutoff wavenumber of the highest mode used in both waveguides is equal. In other words, for any given number of modes, $N1$, which has the highest cutoff wavenumber, $h^{\max}_{mn}$, used in waveguide 1, the number of modes in the elliptic waveguide, $N2$, should be chosen so that all modes having the cutoff wavenumbers equal and smaller than $h^{\max}_{mn}$ are included. In

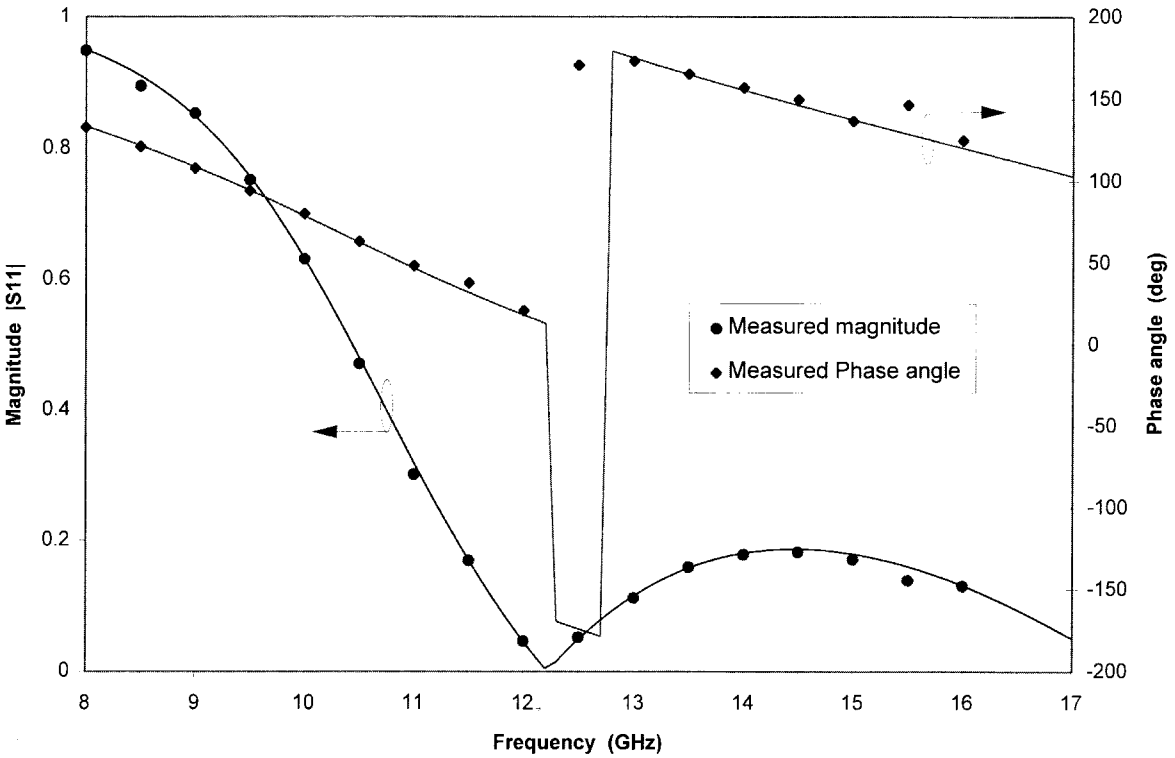

Fig. 4. Calculated and measured reflection coefficient of an elliptic aperture (major $= 18$ mm, minor $= 8$ mm) with thickness of 10 mm inside a X-band rectangular waveguide.

this paper's analysis, such a mode-ratio scheme is also applied to determine the ratio between TE and TM modes used in waveguide 1. Therefore, the number of TE and TM modes used in both waveguides can be uniquely defined by a single value of $h_{mn}^{\max}$.

Table I clearly shows the convergence of the reflection coefficient S_{11} for a rectangular-to-elliptic waveguide junction as a function of the highest cutoff wavenumber in the rectangular waveguide.

VI. Results

To verify this paper's theoretical results, the reflection coefficients of different concentric-elliptic apertures inside a rectangular waveguide have been measured. In the first case, an elliptic aperture of major axis $= 15$ mm and minor axis $= 7$ mm was placed in a standard X-band rectangular waveguide ($a = 22.86$ mm, $b = 10.16$ mm). The theoretical and measured reflection characteristic of the aperture with the thicknesses of 7.5 mm are shown in Fig. 3. One notices good agreement between the two sets of results. The theoretical values were computed using 73 TE and 59 TM modes in the rectangular waveguide, and 27 TE and 19 TM modes in the elliptic waveguide, which corresponds to a $h_{mn}^{\max}$ of 25.

A second elliptic aperture with major axis $= 18$ mm, minor axis $= 8$ mm, and with thickness of 10 mm was placed in a X-band waveguide. Fig. 4 shows the theoretical and measured reflection coefficient, and again, both sets of results show good agreement. In this case, all the modes having a wavenumber smaller than 30 were used. This requires 71 TE and 57 TM modes in the rectangular waveguide, and 36 TE and 27 TM modes in the elliptic waveguide.

For the circular-to-elliptic waveguide junction, this paper's results are compared with a circular-to-circular waveguide junction by using an elliptic waveguide with a very small eccentricity, i.e., the dimension of the major axis is approximately the same as the minor axis. Table II shows the authors' computed results and the measured results presented in [15]. Both sets of results exhibit good agreement. For this junction, $h_{mn}^{\max}$ of 0.8 and 1.2 were used to define the mode ratio, respectively, for the case of the elliptic waveguide with minor axis of 6.35 and 9.525 mm.

TABLE II
Calculated S11 Compared with Measured Results in [15]. Radius of the Larger Circular Waveguide $= 12.74$ mm. The Smaller Circular Waveguide Is Approximated by an Elliptic Waveguide with Eccentricity of 0.04

Thickness (mm.)	frequency GHz)	Reflection Coefficient S11			
		Ref. [15]		Theoretical	
		Magnitude	Phase	Magnitude	Phase
2.54	9	0.956	158.1	0.965	158.4
	12	0.610	118.3	0.615	116.2
5.08	9	0.981	160.6	0.989	160.7
	12	0.803	123.4	0.800	121.3
Radius of the smaller circular waveguide = 6.35mm					
Thickness (mm)	frequency (GHz)	Reflection Coefficient S11			
		Ref. [15]		Theoretical	
		Magnitude	Phase	Magnitude	Phase
2.54	9	0.335	96.6	0.332	96.5
	12	0.033	-99.8	0.032	-114.5
12.7	9	0.701	81.7	0.699	80.9
	12	0.051	161.1	0.036	150.2
Radius of the smaller circular waveguide = 9.525mm					

VII. Conclusion

In this paper, a general solution to the scattering of a waveguide junction having on one side a smaller elliptic waveguide is presented. Closed-form expressions for evaluating coupling integrals

were given to facilitate the use of the mode-matching technique. The expressions can be applied to other geometries as long as their axial field component can be expressed as a Mathieu series—though only rectangular, circular, and elliptic geometries are formulated in this paper. Good agreement between the theoretical and experimental results verifies the analysis presented in this paper.

APPENDIX

Let ψ_i be the solution of the radial-type Mathieu equation, which satisfies the equation

$$\psi_i'' - \left(a_i - \frac{{h_i}^2}{2}\cosh 2u\right)\psi_i = 0 \tag{42}$$

where a_i and h_i is, respectively, the characteristic number and the cutoff wavenumber associated with ψ_i.

Suppose ψ_1 and ψ_2 are, respectively, the solution of

$$\psi_1'' - \left(a_1 - \frac{{h_1}^2}{2}\cosh 2u\right)\psi_1 = 0 \tag{43}$$

and

$$\psi_2'' - \left(a_2 - \frac{{h_2}^2}{2}\cosh 2u\right)\psi_2 = 0. \tag{44}$$

By multiplying (43) by ψ_2 and (44) by ψ_1, one obtains

$$\psi_1''\psi_2 - \left(a_1 - \frac{{h_1}^2}{2}\cosh 2u\right)\psi_1\psi_2 = 0 \tag{45}$$

$$\psi_2''\psi_1 - \left(a_2 - \frac{{h_2}^2}{2}\cosh 2u\right)\psi_1\psi_2 = 0. \tag{46}$$

Subtracting (46) by (45), and integrating with respect to u from 0 to u_o, one gets

$$\int_0^{u_o}\psi_2\psi_1\cosh 2u\,du = \frac{2}{{h_2}^2-{h_1}^2}[\psi_2'\psi_1 - \psi_1'\psi_2]_0^{u_o} - \frac{2(a_2-a_1)}{{h_2}^2-{h_1}^2}\int_0^{u_o}\psi_2\psi_1\,du. \tag{47}$$

From (45), one has

$$[\psi_1'\psi_2]_0^{u_o} - \int_0^{u_o}\psi_1'\psi_2' = a_1\int_0^{u_o}\psi_1\psi_2\,du - \frac{{h_1}^2}{2}\int_0^{u_o}\psi_1\psi_2\cosh 2u\,du. \tag{48}$$

Substituting (47) into (48), yields

$$\int_0^{u_o}\psi_1'\psi_2'\,du = [\psi_1'\psi_2]_0^{u_o} - \frac{{h_2}^2}{{h_2}^2-{h_1}^2}[\psi_2'\psi_1 - \psi_1'\psi_2]_0^{u_o} + \frac{a_2{h_1}^2 - a_1{h_2}^2}{{h_2}^2-{h_1}^2}\int_0^{u_o}\psi_1\psi_2\,du. \tag{49}$$

Following the same procedure, one gets a very similar expression for the circumferential-type Mathieu function ϕ as

$$\int_0^{2\pi}\phi_1'\phi_2'\,du - \left(\frac{a_1{h_2}^2 - a_2{h_1}^2}{{h_2}^2-{h_1}^2}\right)\int_0^{2\pi}\phi_1\phi_2\,du = [\phi_1'\phi_2]_0^{2\pi} - \left(\frac{{h_1}^2}{{h_2}^2-{h_1}^2}\right)[\phi_2'\phi_1 - \phi_1'\phi_2]_0^{2\pi}. \tag{50}$$

Owing to the fact that

$$\phi'(0) = \phi'(2\pi) \quad \text{and} \quad \phi(0) = \phi(2\pi)$$

for both even and odd modes, the right-hand sides of (50) are equal to 0, then

$$\int_0^{2\pi}\phi_1'\phi_2'\,du - \frac{a_1{h_2}^2 - a_2{h_1}^2}{{h_2}^2-{h_1}^2}\int_0^{2\pi}\phi_1\phi_2\,du = 0. \tag{51}$$

ACKNOWLEDGMENT

The authors wish to acknowledge the Department of Electronic Engineering of the University of Hull, for support, Dr. F. A. Alhargan for many helpful discussions on Mathieu functions, and J. Hogdson for making the elliptic apertures.

REFERENCES

[1] J. D. Wade and R. H. Macphie, "Scattering at circular-to-rectangular waveguide junctions," *IEEE Trans. Microwave Theory Tech.*, vol. MTT-34, pp. 1085–1091, Nov. 1986.

[2] R. H. MacPhie and K. L. Wu, "Scattering at the junction of a rectangular waveguide and a larger circular waveguide," *IEEE Trans. Microwave Theory Tech.*, vol. 43, pp. 2041–2045, Sept. 1995.

[3] R. Safavi-Naini and R. H. MacPhie, "On solving waveguide junction scattering problems by the conservation of complex power technique," *IEEE Trans. Microwave Theory Tech.*, vol. MTT-29, pp. 337–343, Apr. 1981.

[4] H. Patzelt and F. Arndt, "Double-plane steps in rectangular waveguides and their application of transformers, irises, and filters," *IEEE Trans. Microwave Theory Tech.*, vol. MTT-30, pp. 771–776, May 1982.

[5] C. Sabatier, "Scattering at an offset circular hole in a rectangular waveguide," *IEEE Trans. Microwave Theory Tech.*, vol. 40, pp. 587–592, Mar. 1992.

[6] R. Bunger P. Martas, and F. Arndt, "Mode-matching analysis of the step discontinuity in elliptical waveguide," *IEEE Microwave Guided Wave Lett.*, vol. 6, pp. 143–145, Mar. 1996.

[7] R. Mittra and S. W. Lee, *Analytical Techniques in the Theory of Guided Waves*. New York: Macmillan, 1971.

[8] T. Itoh, *Numerical Techniques for Microwave and Millimeter-Wave Passive Structure*. New York: Wiley, 1989.

[9] G. G. Gentili, "Properties of TE-TM mode-matching techniques," *IEEE Trans. Microwave Theory Tech.*, vol. 39, pp. 1669–1673, Sept. 1991.

[10] R. Oberhettinger A. Erdelyi, W. Magnus, and F. G. Tricomi, *Higher Transcendental Functions*, vol. III. New York: McGraw-Hill, 1955.

[11] P. M. Morse and H. Feshbach, *Methods of Theoretical Physics*. New York: McGraw-Hill, 1953.

[12] N. W. Mclachlan, *Theory and Application of Mathieu Functions*. London, U.K.: Oxford Univ. Press, 1947.

[13] F. W. Schafke, J. Meixner, and G. Wolf, *Mathieu Functions and Spheroidal Functions and Their Mathematical Foundations*. Berlin, Germany: Springer-Verlag, 1980.

[14] F. Alessabdri, R. Sorrentino, M. Mongiardo, and G. Schiavon, "An investigation of the numerical properties of the mode-matching technique," *Int. J. Numerical Modeling: Electron. Networks, Devices and Fields*, vol. 4, pp. 19–43, 1991.

[15] R. W. Scharstein and A. T. Adams, "Thick circular iris in a TE_{11} mode circular waveguide," *IEEE Trans. Microwave Theory Tech.*, vol. 36, pp. 1529–1531, Nov. 1988.